IEEE Access
Multidisciplinary | Rapid Review | Open Access Journal

Received 1 March 2024, accepted 12 March 2024, date of publication 21 March 2024, date of current version 28 March 2024.

Digital Object Identifier 10.1109/ACCESS.2024.3380456

RESEARCH ARTICLE

Magnetostrictive Vibration Characteristics of Amorphous Alloy Transformer With Three-Dimensional Wound Core

WENLE SONG[1], YU HAN[2], FUYAO YANG[2], JING PANG[3], LEI WANG[1], JIANFEI CAO[4], AND SIYING DENG[5]

[1]State Grid Cangzhou Electric Supply Company, Cangzhou, Hebei 061001, China
[2]State Key Laboratory of Advanced Power Transmission Technology, State Grid Smart Grid Research Institute Company Ltd., Beijing 102211, China
[3]Qingdao Yunlu Advanced Materials Technology Company Ltd., Qingdao, Shandong 266232, China
[4]Hebei Gaojing Electrical Equipment Company Ltd., Handan, Hebei 057150, China
[5]School of Electrical and Electronic Engineering, North China Electric Power University, Beijing 102206, China

Corresponding author: Siying Deng (dengsiying@ncepu.edu.cn)

This work was supported in part by the Technology Project of State Grid Cangzhou Electric Supply Company under Grant KJ2023-058.

ABSTRACT The amorphous alloy transformer with three-dimensional wound core (TDWC) is a new type of transformer structure. Compared with the traditional three-phase five-column transformer with planar wound core (PWC), the TDWC structure exhibits a fully symmetrical magnetic circuit, resulting in enhanced short-circuit withstand capability. However, the vibration noise of the core becomes a significant engineering challenge in the design and manufacturing process due to the larger magnetostrictive coefficient of the amorphous alloy. This study establishes a magnetic-mechanical coupling mathematical model for amorphous alloy TDWC considering the magnetostrictive effect. Three-dimensional finite element analysis (FEA) is adopted to calculate the flux and vibration displacement distribution of the TDWC. Additionally, an experimental validation is conducted on a 200kVA amorphous alloy TDWC prototype to verify the accuracy of the model. Furthermore, a comparison with the PWC prototype demonstrates that the TDWC structure can effectively reduce surface vibrations, and the dominant frequency distribution law of vibration displacement at different positions of the TDWC structure is revealed, providing a foundation for the design of vibration reduction and noise control for TDWC.

INDEX TERMS Amorphous alloy, magnetostriction, planar wound core, three-dimensional wound core, vibration characteristics.

I. INTRODUCTION

Amorphous alloy materials possess excellent properties of high permeability and low loss, which can significantly reduce the transformer no-load loss to achieve an energy-saving effect as shown by [1], [2]. However, the magnetostriction of amorphous alloy material is more significant than that of silicon steel, which leads to more obvious vibration and noise as shown by [3], [4], and [5]. The planar wound core (PWC) and the three-dimensional wound core (TDWC) are the most common core structures of amorphous alloy transformers, and their characteristics are shown in Table 1. Due to the structural difference, the vibration characteristics of the TDWC are pretty different from those of the PWC. Compared with the PWC, the TDWC has the advantages of strong resistance to sudden short circuit, small size, and low cost.

In the past, a series of studies have been carried out on amorphous transformer cores, mainly focusing on three aspects: magnetic properties of the core, magnetostrictive force and vibration characteristics of the core. For magnetic properties of the core, the characteristics of the magnetic density distribution inside PWC and TDWC under different excitation conditions have been investigated respectively as shown by [6] and [7]. For magnetostrictive force, considering the influence of the magnetic permeability by the stress,

The associate editor coordinating the review of this manuscript and approving it for publication was Akshay Kumar Saha.

TABLE 1. Comparison of PWC and TDWC.

Core type	PWC	TDWC
Structure composition	Four single-frame cores arranged in parallel	Three single-frame cores arranged in a triangular shape
Cross-section	Rectangular	Approximately circular
Lengths of magnetic circuits	Unequal	Equal

the force on the core in the electromagnetic field and the change of the internal stress caused by magnetostriction have been researched by the method of imaginary displacement in as shown by [8] and [9]. The finite element analysis (FEA) is carried out for the magneto-mechanical weak coupling problem considering magnetostriction, and the magnetostrictive force is calculated numerically by the elastic mechanics method as shown by [10], [11], and [12]. Simulations of transformer cores have been analyzed in as shown by [13] and [14], and the results show that the magnetostrictive force, rather than the electromagnetic force, is the main factor causing the vibration of the transformer core. For vibration characteristics of the core, the vibration characteristics of single-phase amorphous alloy planar wound cores have been researched under various support boundary conditions [15]. A comparative analysis of the vibration displacement characteristics is performed by constructing a vibration testing platform for single-frame cores, two-frame single-phase transformers, and three-frame three-phase transformers [16].

To sum up, researchers commonly use planar wound core amorphous transformers for analysis and calculation when studying vibration caused by magnetostriction. With advances in manufacturing technology, the attention of users is increasingly drawn towards transformers with novel core structures such as TDWC. However, there is a lack of vibration and noise studies associated with these novel core structures, including the TDWC. The difference between TDWC and PWC regarding vibration displacement characteristics has not been clarified. Studying the vibration characteristics of amorphous alloy transformers with TDWC holds significant engineering and academic importance.

To address the above issues, this study examines two amorphous transformers with a TDWC and a PWC, both with a capacity of 200kVA. The main contributions of this paper are summarized in the following:

1) The FEA is employed to compute and compare the surface displacement vibration of the cores.

2) The experimental platform is established, and the positions are arranged in combination with the core structure. The experiment examines the distribution of vibration displacement for both types of cores, thus validating the accuracy of the simulation.

3) An analysis of the vibration characteristics of the TDWC under different operating conditions is conducted, thus providing a theoretical foundation for the design of vibration reduction and noise control in amorphous transformers.

II. ANALYSIS METHOD

A. MAGNETIZATION AND MAGNETOSTRICTION PROPERTIES OF AMORPHOUS ALLOYS

Accurate magnetic characteristic curve acquisition is an essential source of parameters when analyzing the magnetic and vibration characteristics of amorphous transformer cores under working conditions [17]. The graph in Fig.1 illustrates the B-H curve of the amorphous alloy core.

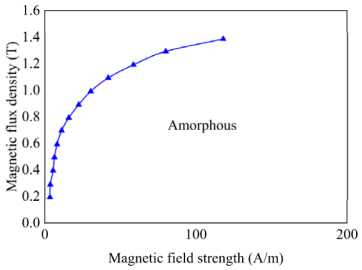

FIGURE 1. Amorphous alloy core magnetization curve.

Magnetostriction is an inherent property of magnetic materials. Under the alternating magnetic field, the size of the amorphous alloy material will change along the magnetization direction due to the magnetostriction, resulting in small deformation [3], so that the amorphous alloy transformer core exhibits periodic vibration twice the excitation frequency. The measured magnetostriction-flux density curve of amorphous alloy strip is shown in Fig.2. λ_pp is the magnetostrictive peak-to-peak value under different flux densities, which can be determined by (1).

$$\lambda_{pp} = \lambda_{max} - \lambda_{min} \tag{1}$$

where λmax and λmin are the maximum elongation and maximum shortening of ferromagnetic materials caused by magnetostriction respectively.

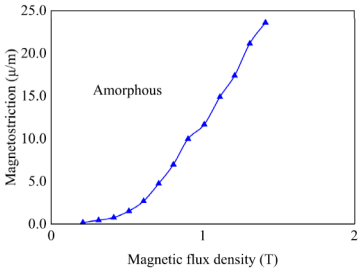

FIGURE 2. Amorphous alloy strip λ_{pp}-B curve.

Through the magnetostrictive peak-to-peak value flux density curve, the magnitude of the deformation caused by the magnetostriction of the transformer core under different flux densities can be obtained so that the stress and vibration acceleration of the core can be calculated.

B. MAGNETIC-MECHANICAL COUPLING MATHEMATICAL MODEL

1) MAGNETIC FIELD EQUATION

This research primarily investigates the vibration characteristics of amorphous transformer cores under power frequency. Therefore, the magnetic field in the core can be regarded as the magnetic quasi-static field, the displacement current can be neglected, and Maxwell's equations can be expressed as follows [3].

$$\nabla \times \boldsymbol{H} = \boldsymbol{J} \tag{2}$$

$$\nabla \times \boldsymbol{E} = -\frac{\partial \boldsymbol{B}}{\partial t} \tag{3}$$

where H is the magnetic field strength; J is the conduction current density; E is the electric field intensity; B is the flux density; t is time.

To simplify the calculation, the vector magnetic potential $\boldsymbol{A}$ is introduced, define $\boldsymbol{B} = \nabla \times \boldsymbol{A}$ and the differential equation of the vector magnetic potential in the core can be obtained by introducing (2).

$$\nabla \times (v\nabla \times \boldsymbol{A}) = \boldsymbol{J} \tag{4}$$

where v is the magnetoresistance rate, which is satisfied $\boldsymbol{H} = v\boldsymbol{B}$, and its value is equal to the reciprocal of the permeability $v = 1/\mu$.

2) MAGNETOSTRICTIVE STRESS

To obtain the magnetostrictive equivalent stress of the core, the amorphous core is integrated in this study, and the interaction between the layers of the amorphous strip is neglected. The magnetostrictive strain is equivalent to the magnetostrictive stress using the stress-strain relationship of elastic mechanics as shown by [18], [19], and [20]. Then, it is calculated and analyzed as a body load. The matrix form of the three-dimensional stress-strain relationship is as follows.

$$\boldsymbol{\sigma} = D\boldsymbol{\varepsilon} \tag{5}$$

where σ is the stress vector; ε is the strain vector; **D** is an elastic matrix, and its expression is as follows.

$$D = \frac{E(1-\alpha)}{(1+\alpha)(1-2\alpha)} \begin{bmatrix} 1 & \frac{a}{1-\alpha} & \frac{a}{1-\alpha} & 0 & 0 & 0 \\ \frac{a}{1-\alpha} & 1 & \frac{a}{1-\alpha} & 0 & 0 & 0 \\ \frac{a}{1-\alpha} & \frac{a}{1-\alpha} & 1 & 0 & 0 & 0 \\ 0 & 0 & 0 & \frac{1-2\alpha}{2(1-\alpha)} & 0 & 0 \\ 0 & 0 & 0 & 0 & \frac{1-2\alpha}{2(1-\alpha)} & 0 \\ 0 & 0 & 0 & 0 & 0 & \frac{1-2\alpha}{2(1-\alpha)} \end{bmatrix} \tag{6}$$

where $\boldsymbol{E}$ is Young's modulus; α is the Poisson's ratio of the material.

From (5) and (6), the magnetostrictive stress of the three-dimensional wound core can be calculated, and then the magnetostrictive volume force can be obtained by introducing (7).

$$\nabla \cdot \boldsymbol{\sigma} = -\boldsymbol{F}_{\mathrm{v}} \tag{7}$$

where $\boldsymbol{F}_{\mathrm{v}}$ is the magnetostrictive body force.

3) VIBRATION EQUATION

Ignoring the damping impact of the core, the differential equation of the structural force field is as follows.

$$\boldsymbol{M}\frac{\mathrm{d}^2\boldsymbol{u}}{\mathrm{d}t^2} + \boldsymbol{K}\boldsymbol{u} = \boldsymbol{F}_{\mathrm{v}} \tag{8}$$

where $\boldsymbol{M}$ is the mass matrix; $\boldsymbol{K}$ is the stiffness matrix; $\boldsymbol{u}$ is the displacement vector.

By solving (8), the vibration displacement vector of the core can be calculated, and the overall vibration of the core can be obtained.

III. SIMULATION OF PWC AND TDWC

A. MODEL ESTABLISHMENT

To verify the accuracy of the measured magnetic properties data of the amorphous alloy and better analyze and predict the vibration of the amorphous alloy transformer core, the 3-D FEA model is established for the amorphous alloy PWC and the TDWC. The extraction positions for vibration displacement data on the surface of each core during simulation, labeled as positions A, B, and C, are illustrated in Fig.3 and Fig.4.

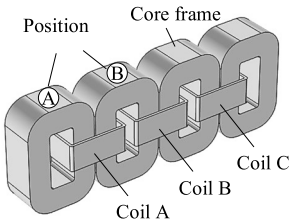

FIGURE 3. Three-phase four-frame five-column PWC model.

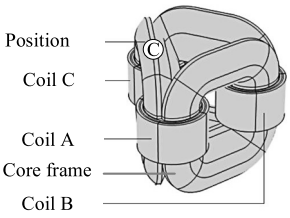

FIGURE 4. TDWC model.

To compare the vibration characteristics of the amorphous alloy PWC and TDWC, the flux density value of the core column is set to 1.2 T, and the vibration displacement characteristics of the core surface are calculated respectively. The parameters of the amorphous alloy core are shown in Table 2. The coil is made of copper wire and filled with air around the core.

TABLE 2. Simulation parameter.

Parameter	Unit	Value	
		PWC	TDWC
Effective cross-section area of core column	m^2	0.031	0.033
The number of turns of excitation coil	Turns	25	10
Flux density	T	1.2	1.2
Effective value of excitation voltage	V	220	83.47
Poisson 's ratio of core	/	0.3	0.3
Core Young's modulus	GPa	110	110

B. FLUX DENSITY AND VIBRATION DISPLACEMENT OF PWC AND TDWC

Fig.5(a) and (b) show the flux density distribution calculation diagram of the PWC and the TDWC model at 13 ms time along the z-direction section of the core frame. The chart shows that the flux density of the two cores is more significant at the inner corner of the core and more minor at the outer corner of the core. The flux density distribution inside the core column and the upper yoke is relatively uniform, and the average flux density in this area is 1.2 T.

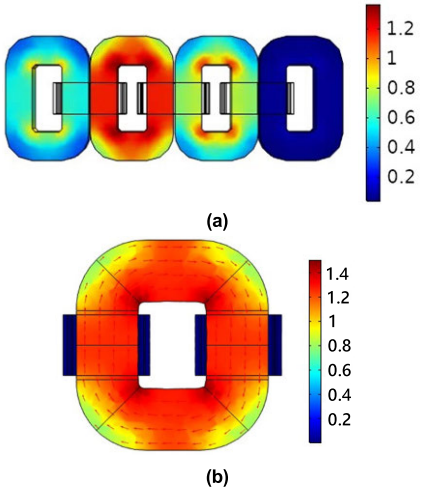

FIGURE 5. Flux distribution map of the core. (a) PWC. (b) The single core frame of the TDWC.

Using the solid mechanics module of COMSOL software, and inputting the magnetostrictive-magnetic flux density curve of the amorphous alloy into the module, the surface displacement distribution of the core is calculated. As shown in Fig.6, the surface vibration displacement of the two cores gradually decreases from the upper part to the lower part of the core. The average vibration displacement amplitude of the upper surface of the core is the largest, and the vibration amplitude of the left and right core columns is the same, symmetrically distributed on both sides of the core frame. The maximum vibration of the PWC and the TDWC is located at the corner of the upper iron yoke and the core column, reaching 6.28×10^{-6} m and 2.1×10^{-6} m respectively.

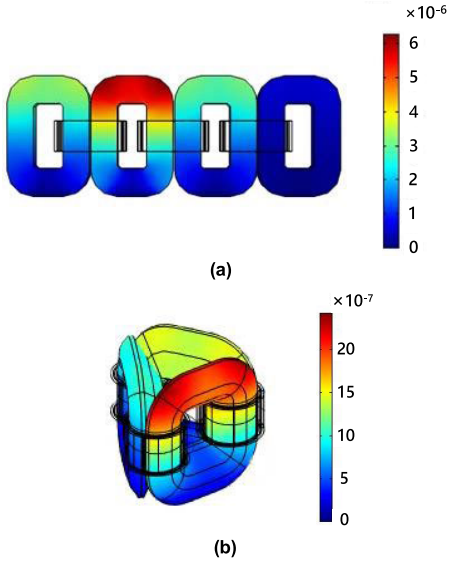

FIGURE 6. Distribution of vibration displacement on the core surface. (a) PWC. (b) TDWC.

The simulation values of the vibration displacement on the upper surface of the TDWC and the PWC are compared, as shown in Fig.7. It can be obtained that under the same flux density, the vibration displacement amplitude of the PWC is greater than that of the TDWC. The vibration of the PWC structure will be more severe, and the noise will be greater. The TDWC configuration can diminish surface vibrations in the core, thereby mitigating the noise generated by the amorphous alloy transformer to a certain extent.

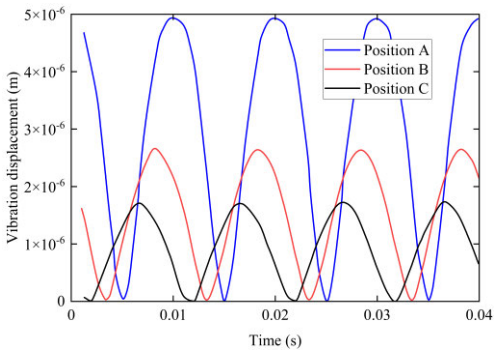

FIGURE 7. Comparison of vibration displacement simulation values of TDWC and PWC.

IV. CORE VIBRATION DISPLACEMENT EXPERIMENT

A. EXPERIMENTAL COMPARISON BETWEEN PWC AND TDWC

To further study the vibration characteristics of amorphous alloy transformer cores with different structures and verify the correctness of the vibration displacement calculated by the simulation model, the vibration experiments of the PWC and the TDWC are carried out respectively. The experimental prototype is shown in Fig.8. The amplitude of the applied three-phase AC supply is the same as the simulation value,

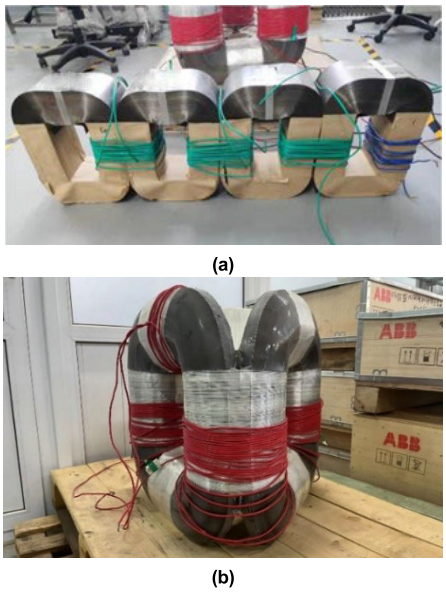

FIGURE 8. Experimental site. (a) PWC. (b) TDWC.

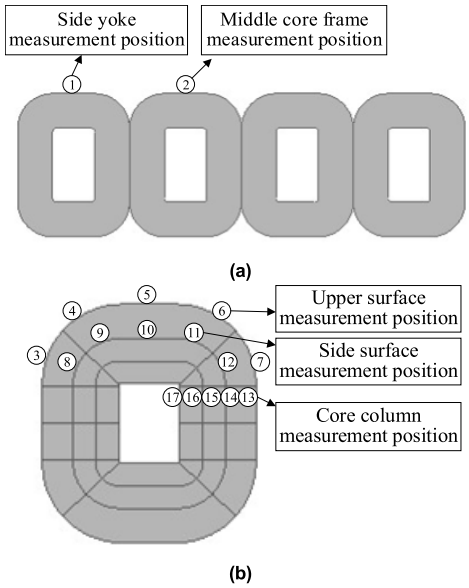

FIGURE 9. Layout of surface vibration measurement positions. (a) PWC. (b) The single core frame of the TDWC.

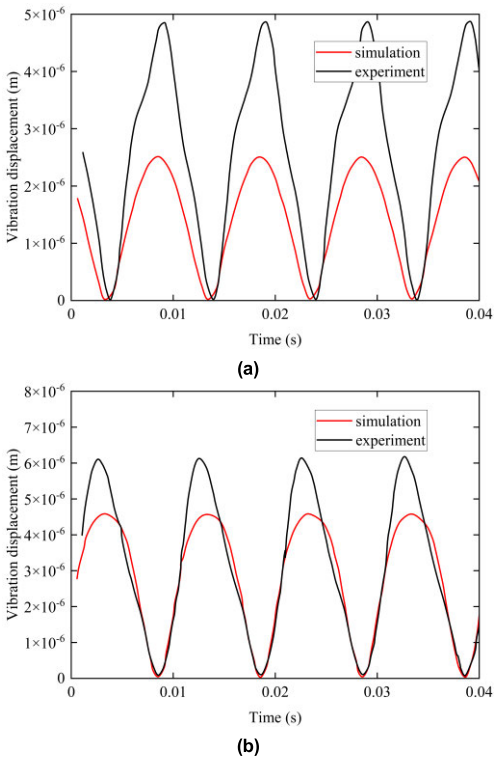

FIGURE 10. Comparison of vibration displacement simulation and experiment of the PWC. (a) Measurement position 1. (b) Measurement position 2.

which is 220 V and 83.47 V respectively, and the frequency is 50 Hz. The number of excitation coils is the same as the simulation value, which is 10 turns and 25 turns.

A three-phase programmable power supply is used to provide power frequency voltage for the core, a power analyzer is used to observe and record the applied excitation signal, and a piezoelectric vibration acceleration sensor is used to measure the vibration of the core surface and record the data to the computer.

Since the acceleration sensor measures the vibration in the thickness direction of the rectangular cross-section of the PWC, and the measurement result is one order of magnitude smaller than the upper surface, the influence on the vibration amplitude of the entire core is relatively small. Therefore, the measurement positions are only arranged on the upper surface of the side yoke and the middle core frame of PWC, as shown in positions 1 and 2 in Fig.9(a). For the TDWC with a nearly semi-circular cross-section on the upper yoke, the vibration exhibits a superposition effect on the upper yoke, and the three core frames have a completely symmetrical structure. Therefore, the vibration measurement positions only need to be arranged on one core frame. The corresponding measurement positions on the upper yoke upper surface are $3 \sim 7$, on the upper yoke side surface are $8 \sim 12$, and on the core column are $13 \sim 17$, as shown in Fig.9(b).

Comparing the vibration displacement simulation value and the experimental value of the measurement position of the PWC, as shown in Fig.10, it can be observed that the vibration displacement of the middle core frame (Position 2) is greater than that of the side yoke core frame (Position 1). Additionally, the simulated values are lower than the experimental values. This discrepancy can be ascribed to the impact of the production process of the PWC, which results in uneven distribution of gaps in the upper yoke. Consequently, the presence of these uneven gaps amplifies the vibration displacement of the core. However, the simulation model does not account for the impact of the gaps in the upper yoke.

The simulation values and experimental values of the vibration displacement of the upper surface central position (Position 5) and the core column measurement position

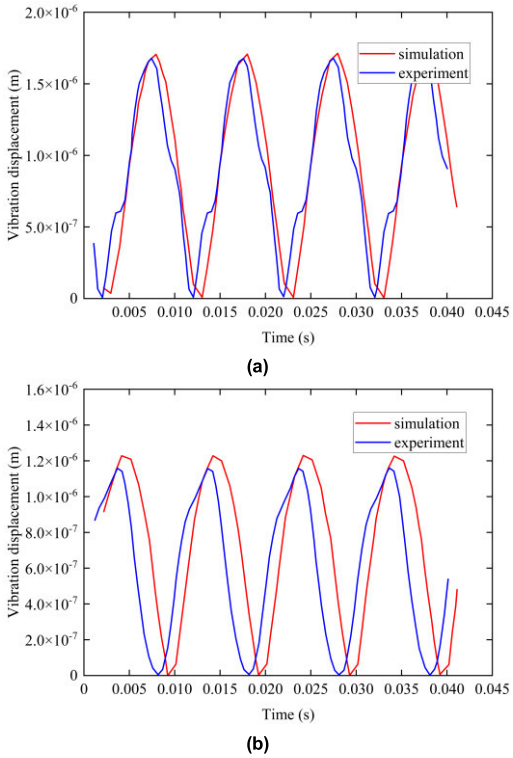

FIGURE 11. Simulation and test comparison of TDWC vibration displacement. (a) Measurement position 5. (b) Measurement position 14.

(Position 14) of the TDWC are compared, as shown in Fig.11. It can be observed that the simulated vibration displacement waveform closely matches the experimental values with minor errors. This can be attributed to the fact that the TDWC structure generally adopts a closed core configuration, where the layers of strip materials are tightly compressed, resulting in fewer internal gaps within the core. Therefore, the Maxwell electromagnetic force in the air gap can be ignored, and the primary cause of core vibration is considered to be the magnetostrictive force induced by the magnetostrictive effect of the amorphous alloy material.

Regarding the core column position, the simulated vibration displacement results are higher than the experimental test results. The omission of the contact between the coil and the core in the simulation can explain this discrepancy. In contrast, during the experiment, the core column was surrounded by coil windings, which can influence the vibration testing results of the core column to some extent.

Combined with Fig.10 and 11, it can be seen that the TDWC can reduce the surface vibration of the core compared with the PWC. The vibration displacement amplitudes of the upper surface of the PWC and the TDWC are 6.2×10^{-6} m (Position 2) and 1.7×10^{-6} m (Position 5), respectively. Due to the structural difference of the core, the vibration displacement amplitude of the TDWC is quite different from that of the PWC, so the vibration characteristics of the amorphous alloy TDWC need to be further analyzed.

B. ANALYSIS OF VIBRATION CHARACTERISTICS OF THE TDWC

During the vibration experiment, the flux density in the core column is 0.8 T, 0.9 T, 1.0 T, 1.1 T, 1.2 T, and the effective values of the corresponding applied voltage are 146 V, 165 V, 182V, 201 V, and 220 V, respectively.

The vibration acceleration data of the measurement position measured by the piezoelectric acceleration sensor are integrated twice to obtain the vibration displacement of the position. The vibration displacement amplitude of each position is averaged as the vibration displacement amplitude of the position under different excitation voltages, as shown in Fig.12.

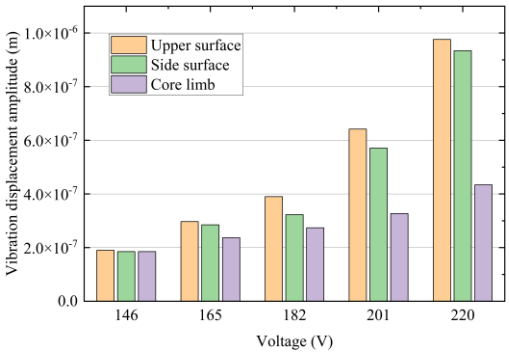

FIGURE 12. Vibration of each position of the TDWC.

From Fig.12, the following points have been observed:

1) The average vibration amplitude is highest on the upper surface of the core and lowest on the core column. When the voltage is 220 V, the average amplitudes on the upper surface and core column are approximately 9.7×10^{-7} m and 4.4×10^{-7} m, respectively.

2) The upper surface of the core is narrower compared to other positions of the core, and the vibration measurement position is parallel to the surface of the coiled amorphous strip. In the vertical direction, the vibrations exhibit a superposition effect, hence resulting in the maximum vibration amplitude on the upper yoke of the amorphous core.

1) ANALYSIS OF VIBRATION CHARACTERISTICS ON THE UPPER SURFACE OF THE CORE

The vibration results of five measurement positions on the upper surface are shown in Fig.13. Under different voltage excitations, the vibration displacement amplitudes of the measurement positions exhibit a symmetrical distribution. As the excitation voltage increases, the vibrations at positions 4 and 6 become more pronounced, resulting in larger displacement amplitudes. At an excitation voltage of 220 V, the vibration displacement amplitudes at positions 4 and 6 can reach 1.9×10^{-6} m, the vibration displacement amplitude at positions 3 is approximately 1.7×10^{-6} m, whereas the displacements at positions 3 and 7 are smaller, approximately 1.5×10^{-6} m.

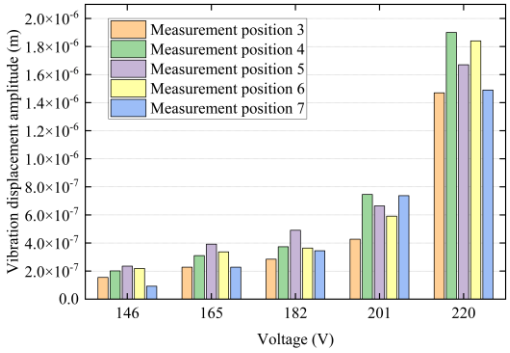

FIGURE 13. Vibration displacement amplitude on the upper surface of the core.

The vibration acceleration spectrum of the central measurement position 5 on the upper surface of the core under different excitation voltages is shown in Fig.14. As the excitation voltage increases, the proportion of the high-frequency component of the vibration acceleration increases correspondingly. When the excitation voltage reaches 220 V, flux density inside the iron yoke approaches saturation. The dominant vibration frequencies are 100 Hz, 300 Hz and 400 Hz, with the highest vibration frequency component reaching 500 Hz.

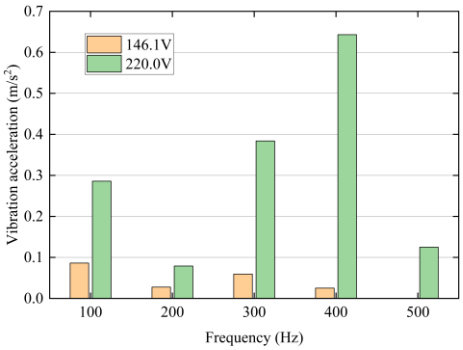

FIGURE 14. Measurement position 5 vibration acceleration spectrum.

For measurement position 5, the 100 Hz, 200 Hz, 300 Hz and 400 Hz components with high vibration acceleration spectrum are taken for analysis, and their relationship with voltage is shown in Fig.15. It can be obtained:

a) The vibration acceleration component at 100 Hz demonstrates a direct proportionality to the voltage. In contrast, the 200Hz component initially increases with rising voltage, then decreases, reaching only 0.07×10^{-6} m at 220 V.

b) The growth rates of the vibration acceleration components at 300 Hz and 400 Hz gradually accelerate with increasing voltage, eventually becoming the dominant frequencies of the vibration acceleration. At 220 V, they can peak at 0.39×10^{-6} m and 0.65×10^{-6} m, respectively. Therefore, when implementing vibration reduction measures at the central position 5, consideration should be given to the 300 Hz and 400 Hz components.

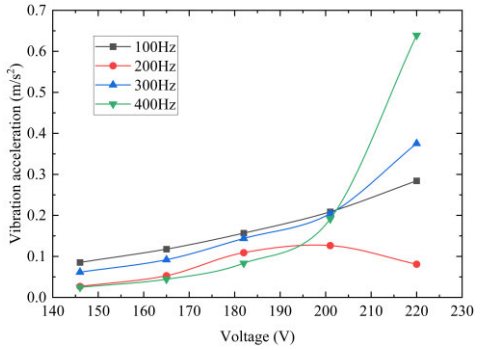

FIGURE 15. Relationship between vibration acceleration and voltage of measurement position 5 on the upper surface of the core.

2) ANALYSIS OF VIBRATION CHARACTERISTICS ON THE SIDE SURFACE OF THE CORE

When the excitation voltage is 146 V and 220 V, the vibration displacement amplitude of the measurement positions 8∼12 on the side surface is shown in Fig.16. It can be observed that at lower excitation voltage amplitudes, the differences in vibration displacement amplitudes among the measurement positions on the lateral surface of the core are minimal.

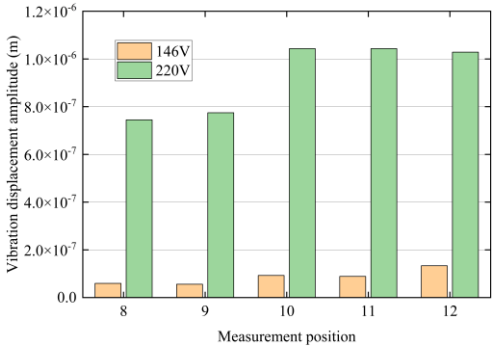

FIGURE 16. Vibration displacement amplitude on the side surface of the core.

The acceleration spectrum of vibrations at the central measurement position 10, located on the lateral surface of the core, is depicted in Fig.17 for various excitation voltages. It can be observed that under the same excitation voltage, the vibration acceleration amplitudes on the side surface are slightly smaller than those on the upper surface of the yoke. The dominant frequency of the vibration acceleration of the measurement position is 100 Hz.

For measurement position 10, the 100 Hz, 200 Hz and 300 Hz components with high vibration acceleration spectrum are taken for analysis, and their relationship with voltage is shown in Fig.18. It can be obtained:

a) All spectral components increase with the rise in excitation voltage. Particularly, the growth rate of the 300 Hz component accelerates gradually, indicating that as flux density approaches saturation, higher-frequency vibration displacement spectrum components become more prominent.

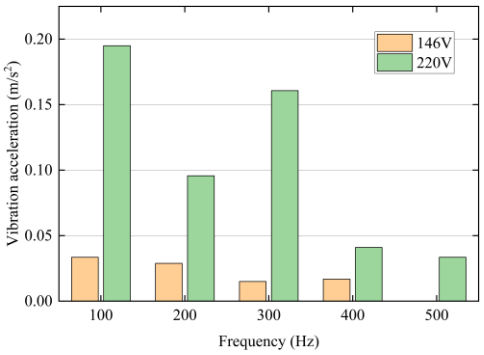

FIGURE 17. Side surface measurement position 10 vibration acceleration spectrum.

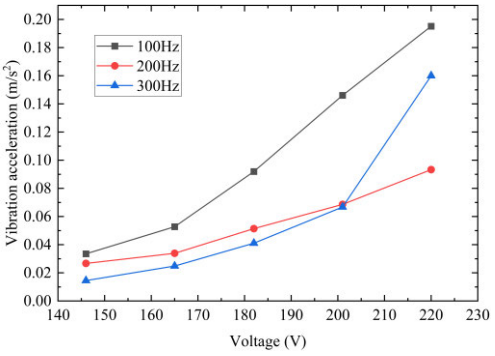

FIGURE 18. Relationship between vibration acceleration and voltage of measurement position 10 on the side surface of the core.

b) The differences in amplitude of the vibration acceleration spectral components on the side surface are relatively small. When the excitation voltage reaches 220 V, the vibration acceleration amplitudes of the 100 Hz, 200 Hz, and 300 Hz components are approximately 0.2×10^{-6} m, 0.1×10^{-6} m, and 0.16×10^{-6} m, respectively.

3) ANALYSIS OF VIBRATION CHARACTERISTICS OF THE CORE COLUMN

The vibration displacement amplitude of each measurement position on the core column under different excitation voltages is shown in Fig.19. The position 13 located on the outer side of the core column exhibits significantly larger vibration displacement amplitudes compared to positions 15 and 16 located in the middle of the core column, and this difference becomes more pronounced as the voltage increases. Additionally, when the magnetic induction intensity inside the core column reaches saturation, the vibration displacement amplitude at position 17 located on the inner side of the core column increases significantly.

There is a significant difference in vibration amplitude between the inner and outer regions of the core column, resulting in different vibration characteristics. A comparison of the vibration acceleration spectrum at position 13 on the outer side and position 17 on the inner side of the core column is shown in Fig.20. The dominant frequency of vibration

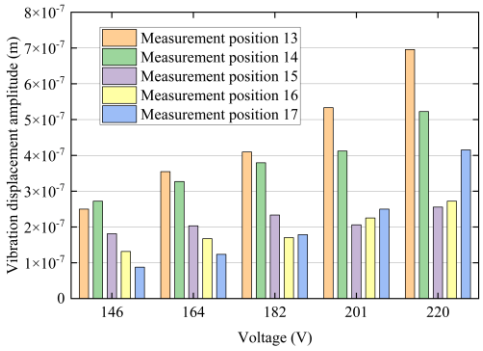

FIGURE 19. Vibration displacement amplitude of the core column.

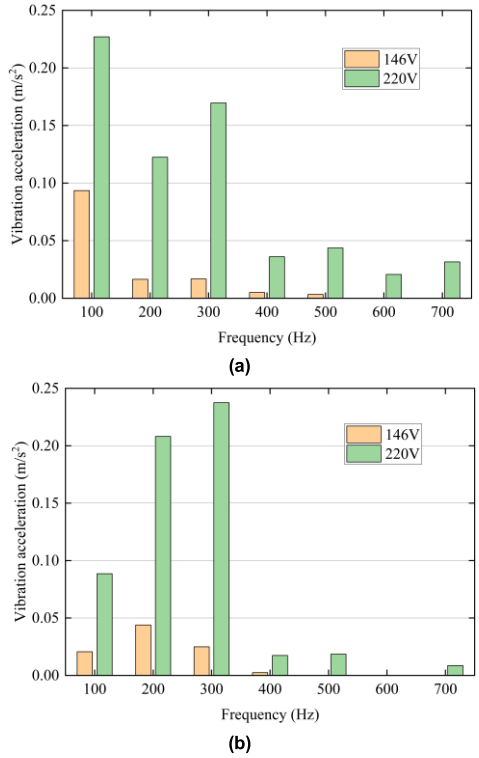

FIGURE 20. Vibration acceleration spectrum of measurement positions of the core column. (a) Measurement position 13. (b) Measurement position 17.

acceleration at position 13 is 100 Hz, whereas at position 17, it is 200 Hz, with a relatively lower proportion of the 100 Hz component.

Taking the vibration acceleration spectrum components at 100Hz, 200Hz, and 300Hz into consideration, the relationship between vibration acceleration and voltage at measurement positions 13 and 17 is illustrated in Fig.21. It can be obtained:

a) For position 13, although the growth rates of the vibration acceleration components at 200 Hz and 300 Hz increase gradually, the dominant frequency of vibration acceleration remains at 100 Hz. When the excitation voltage is 220 V, the vibration acceleration amplitude is maximized

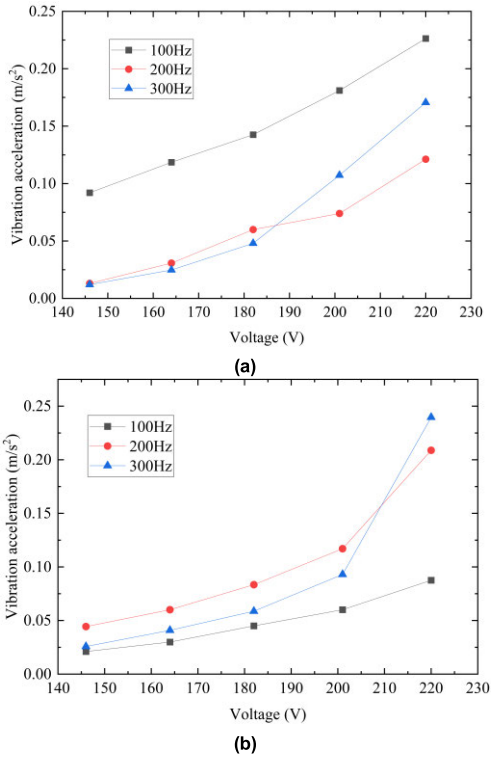

FIGURE 21. Relationship between vibration acceleration and voltage of measurement positions of the core column. (a) Measurement position 13. (b) Measurement position 17.

for the 100 Hz component, at approximately 0.23×10^{-6} m, while the 200 Hz component is minimized, at around 0.13×10^{-6} m.

b) For position 17, the vibration acceleration at the 200 Hz component is the highest. As the voltage increases, the 300 Hz component gradually becomes the highest contributor to the vibration acceleration. When the excitation voltage is 220 V, the vibration acceleration amplitude is maximized for the 300 Hz component, at approximately 0.24×10^{-6} m, while the 100Hz component is minimized, at around 0.09×10^{-6} m.

Therefore, on the same horizontal plane, the vibration displacement amplitude increases as it gets closer to the outer side of the core column. For the outer side of the core column, the dominant vibration frequency is 100 Hz; whereas for the inner side of the core column, due to its shorter magnetic path length and higher flux density, under higher excitation voltages, the nonlinear magnetostrictive properties of the material have a greater impact, resulting in a significant proportion of the 200 Hz and 300 Hz components in the vibration spectrum.

V. CONCLUSION

This study presents a novel FEA model for the amorphous transformer with TDWC, based on the theory of magnetic-mechanical coupling. Subsequently, an experimental platform is constructed to acquire the vibration displacement distribution on the core surface. Furthermore, an in-depth analysis of the vibration characteristics of the TDWC under various operating conditions is conducted. The main conclusions can be drawn as follows:

1) The TDWC exhibits a gradual decrease in surface vibration displacement from the upper part to the lower part, with the maximum average vibration displacement amplitude observed on the upper surface of the core. Under the same flux density, the vibration displacement amplitude of the TDWC is smaller than that of PWC. Experimental results show that at a working flux density of 1.2 T, the vibration displacement amplitudes on the upper surfaces of the TDWC and the PWC are 1.7×10^{-6} m and 6.2×10^{-6} m respectively. The use of a TDWC structure can reduce surface vibrations to some extent.

2) With increasing excitation voltage, the proportion of high-frequency components in vibration displacement at various positions on the core surface also increases correspondingly. For the upper surface of the TDWC, the dominant vibration frequency is 100 Hz. When the excitation voltage exceeds 200 V, 300 Hz and 400Hz become the dominant frequencies of vibration acceleration. For the side surface of the core, the vibration acceleration amplitude is slightly smaller than that of the upper surface, with minor differences in vibration displacement amplitudes at each measuring position. The dominant vibration frequency is 100 Hz. For the core column, the vibration displacement amplitudes increase closer to the outer side. The dominant vibration frequency on the outer side of the core column is 100 Hz, while the inner side is more affected by the magnetostrictive nonlinear characteristics of material, with a dominant vibration frequency of 200 Hz.

In future research, it is imperative to conduct further investigations on the sound field distribution surrounding the amorphous transformer with TDWC, evaluate the operational noise level of the transformer, and explore the optimization method for reducing the transformer noise.

REFERENCES

[1] J. E. Gao, H. X. Li, Z. B. Jiao, Y. Wu, Y. H. Chen, T. Yu, and Z. P. Lu, "Effects of nanocrystal formation on the soft magnetic properties of Fe-based bulk metallic glasses," *Appl. Phys. Lett.*, vol. 99, no. 5, Aug. 2011, Art. no. 052504.

[2] J. Zhang, R. Cui, Y. Wei, D. Yu, S. Xie, S. Fang, and J. Shen, "Optimization and experimental validation of amorphous alloy high-speed asynchronous motor for simultaneous reduction on core and copper losses," *IEEE Access*, vol. 11, pp. 101112–101122, 2023.

[3] Y. Li, Z. Yang, C. Zhang, and S. Mu, "Vibration and noise measurement of medium-high frequency transformer cores under non-sinusoidal excitation," *IEEE Trans. Magn.*, vol. 58, no. 8, pp. 1–5, Aug. 2022.

[4] L. Zhu, J. Hao, and L. Lu, "Research on influence of damping on the vibration noise of transformer," *IEEE Access*, vol. 10, pp. 92128–92136, 2022.

[5] P. Zhang and L. Li, "Vibration and noise characteristics of high-frequency amorphous transformer under sinusoidal and non-sinusoidal voltage excitation," *Int. J. Electr. Power Energy Syst.*, vol. 123, Dec. 2020, Art. no. 106298.

[6] D. Liu, J. Li, R. K. Noubissi, S. Wang, X. Xu, and Q. Liu, "Magnetic properties and vibration characteristics of amorphous alloy strip and its combination," *IET Electr. Power Appl.*, vol. 13, no. 10, pp. 1589–1597, Jul. 2019.

[7] B. X. Du and D. S. Liu, "Dynamic behavior of magnetostriction-induced vibration and noise of amorphous alloy cores," *IEEE Trans. Magn.*, vol. 51, no. 4, pp. 1–8, Apr. 2015.

[8] O. A. Mohammed, S. Liu, and N. Abed, "Study of the inverse magnetostriction effect on machine deformation," in *Proc. IEEE SoutheastCon*, Greensboro, NC, USA, Jun. 2004, pp. 433–436.
[9] K. A. Fonteyn, A. Belahcen, P. Rasilo, R. Kouhia, and A. Arkkio, "Contribution of Maxwell stress in air on the deformations of induction machines," *J. Electr. Eng. Technol.*, vol. 7, no. 3, pp. 336–341, May 2012.
[10] K. Delaere, W. Heylen, K. Hameyer, and R. Belmans, "Local magnetostriction forces for finite element analysis," *IEEE Trans. Magn.*, vol. 36, no. 5, pp. 3115–3118, Sep. 2000.
[11] M. Besbes, Z. Ren, and A. Razek, "Finite element analysis of magneto-mechanical coupled phenomena in magnetostrictive materials," *IEEE Trans. Magn.*, vol. 32, no. 3, pp. 1058–1061, May 1996.
[12] T. Hilgert, L. Vandevelde, and J. Melkebeek, "Comparison of magnetostriction models for use in calculations of vibrations in magnetic cores," *IEEE Trans. Magn.*, vol. 44, no. 6, pp. 874–877, Jun. 2008.
[13] P. Zhang, L. Li, Z. Cheng, C. Tian, and Y. Han, "Study on vibration of iron core of transformer and reactor based on Maxwell stress and anisotropic magnetostriction," *IEEE Trans. Magn.*, vol. 55, no. 2, pp. 1–5, Feb. 2019.
[14] S. Wu, W. Li, W. Tong, and R. Tang, "Electromagnetic vibration and noise comparison of amorphous metal PMSMs and silicon steel PMSMs," *IEEE Access*, vol. 7, pp. 62672–62680, 2019.
[15] T. Mizuta, Y. Tani, and K. Fujiwara, "Magnetic property of amorphous magnetic thin ribbon and its laminated bulk under tensile and compressive stresses," *IEEE Trans. Magn.*, vol. 54, no. 11, pp. 1–5, Nov. 2018.
[16] Y.-H. Chang, C.-H. Hsu, H.-L. Chu, and C.-P. Tseng, "Magnetomechanical vibrations of three-phase three-leg transformer with different amorphous-cored structures," *IEEE Trans. Magn.*, vol. 47, no. 10, pp. 2780–2783, Oct. 2011.
[17] X. Zhou and L. Zhu, "Magnetostrictive simulation of amorphous alloy based on dynamic Jiles–Atherton model," in *Proc. FAFEE*. Singapore: Springer, 2021, pp. 765–774.
[18] D. Liu, B. Du, M. Yan, and S. Wang, "Suppressing noise for an HTS amorphous metal core transformer by using microperforated panel absorber," *IEEE Trans. Appl. Supercond.*, vol. 26, no. 7, pp. 1–5, Oct. 2016.
[19] Z. Lihua, L. Jingjing, Y. Qingxin, Z. Jianguo, and C.-S. Koh, "An improved magnetostriction model for electrical steel sheet based on Jiles–Atherton model," *IEEE Trans. Magn.*, vol. 56, no. 3, pp. 1–4, Mar. 2020.
[20] M. Liu, O. Hubert, X. Mininger, F. Bouillault, L. Bernard, and T. Waeckerlé, "Reduction of power transformer core noise generation due to magnetostriction-induced deformations using fully coupled finite-element modeling optimization procedures," *IEEE Trans. Magn.*, vol. 53, no. 8, pp. 1–11, Aug. 2017.

WENLE SONG received the M.E. degree in electrical engineering from Beijing Jiaotong University, Beijing, China, in 2013.

He is currently a Senior Engineer (S.E.) with State Grid Cangzhou Electric Supply Company, Cangzhou, China. He has three provincial and ministerial level scientific and technological progress awards, authorized five invention patents, and published six articles.

YU HAN received the B.E. and M.E. degrees in materials processing engineering from Wuhan University (WHU), Hubei, China, in 2002 and 2005, respectively, and the Ph.D. degree in power mechanical engineering from North China Electric Power University (NCEPU), Beijing, China, in 2017.

She is currently a Research and Development Engineer with the State Key Laboratory of Advanced Power Transmission Technology, State Grid Smart Grid Research Institute Company Ltd. Her research interests include electrical and magnetic materials, electrical machines, and wireless power transfer.

FUYAO YANG received the B.E. and M.E. degrees in materials science and engineering from Harbin Institute of Technology (HIT), Harbin, China, in 2008 and 2010, respectively, and the Ph.D. degree in materials science from the University of Science and Technology Beijing (USTB), Beijing, China, in 2018.

He is currently a Research and Development Engineer with the State Key Laboratory of Advanced Power Transmission Technology, State Grid Smart Grid Research Institute Company Ltd. His research interests include electrical and magnetic materials, electrical machines, and wireless power transfer.

JING PANG received the Ph.D. degree in electrical engineering from Shenyang University of Technology (SUT), Shenyang, China, in 2019.

He is currently a Senior Engineer (S.E.) with Qingdao Yunlu Advanced Materials Technology Company Ltd. He has five provincial and municipal science and technology awards, authorized 56 invention patents, and published ten articles. His research interests include the development and application of soft magnetic materials.

LEI WANG received the M.E. degree in electrical engineering from Northeast Electric Power University (NEEPU), Jilin, China, in 2012, and the Ph.D. degree in electrical engineering from South China University of Technology (SCUT), Canton, China, in 2018.

He is currently a Senior Engineer (S.E.) with State Grid Cangzhou Electric Supply Company, Cangzhou, China. He authorized five invention patents and published six articles. His research interest includes distribution network primary equipment operation management technology.

JIANFEI CAO received the B.E. degree in electrical engineering from Shenyang University of Technology (SUT), Shenyang, China, in 1999.

He is currently a Senior Engineer (S.E.) with Hebei Gaojing Electrical Equipment Company Ltd. He was involved in the development and revision of several national and local standards, including GB/T 6451-2023 "technical parameters and requirements for oil-immersed power transformers" and Hebei provincial local standard DB13/T 2201-2015 "specification and technical requirements for three-phase oil-immersed tridimensional toroidal-core distribution transformers."

SIYING DENG received the B.E. degree in electrical engineering and automation from China Three Gorges University (CTGU), Yichang, China, in 2020. She is currently pursuing the Ph.D. degree in electrical engineering with the School of Electrical and Electronic Engineering, North China Electric Power University (NCEPU).

Her research interests include the refined design and multi-physical field simulation of high frequency transformer.